Title

Optogenetic EB1 inactivation shortens metaphase spindles by disrupting cortical force-producing interactions with astral microtubules

Journal

Current Biology, 32(5)

ISSN

0960-9822

Authors

Dema, Alessandro
van Haren, Jeffrey
Wittmann, Torsten

Publication Date

2022-03-01

DOI

10.1016/j.cub.2022.01.017

Peer reviewed

HHS Public Access

Author manuscript

Curr Biol. Author manuscript; available in PMC 2023 March 14.

Published in final edited form as:

Curr Biol. 2022 March 14; 32(5): 1197–1205.e4. doi:10.1016/j.cub.2022.01.017.

Optogenetic EB1 inactivation shortens metaphase spindles by disrupting cortical force-producing interactions with astral microtubules

Alessandro Dema[1], **Jeffrey van Haren**[2], **Torsten Wittmann**[1,*]

[1]Department of Cell & Tissue Biology, University of California San Francisco, 513 Parnassus Avenue, San Francisco, CA 94143

[2]Department of Cell Biology, Erasmus MC, Rotterdam, The Netherlands

SUMMARY

Chromosome segregation is accomplished by the mitotic spindle, a bipolar micromachine built primarily from microtubules. Different microtubule populations contribute to spindle function: Kinetochore microtubules attach and transmit forces to chromosomes, antiparallel interpolar microtubules support spindle structure, and astral microtubules connect spindle poles to the cell cortex.[1,2] In mammalian cells, End Binding (EB) proteins associate with all growing microtubule plus ends throughout the cell cycle and serve as adaptors for diverse +TIPs that control microtubule dynamics and interactions with other intracellular structures.[3] Because binding of many +TIPs to EB1 and thus microtubule-end association is switched off by mitotic phosphorylation[4–6] the mitotic function of EBs remains poorly understood. To analyze how EB1 and associated +TIPs on different spindle microtubule populations contribute to mitotic spindle dynamics, we use a light sensitive EB1 variant, π-EB1, that allows local, acute and reversible inactivation of +TIP association with growing microtubule ends in live cells.[7] We find that acute π-EB1 photoinactivation results in rapid and reversible metaphase spindle shortening and transient relaxation of tension across the central spindle. However, in contrast to interphase, π-EB1 photoinactivation does not inhibit microtubule growth in metaphase, but instead increases astral microtubule length and number. Yet, in the absence of EB1 activity astral microtubules fail to engage the cortical dynein/dynactin machinery and spindle poles move away from regions of π-EB1 photoinactivation. In conclusion, our optogenetic approach reveals mitotic EB1 functions that remain hidden in genetic experiments likely due to compensatory molecular systems regulating vertebrate spindle dynamics.

*Lead contact and correspondence: torsten.wittmann@ucsf.edu; https://twitter.com/WittmannTorsten.

AUTHOR CONTRIBUTIONS

Conceptualization, A.D., J.v.H. and T.W.; Methodology, A.D., J.v.H. and T.W.; Software, T.W.; Investigation, A.D. and J.v.H.; Writing – Original Draft, A.D. and T.W.; Writing – Review & Editing, A.D., J.v.H., and T.W.; Funding Acquisition, T.W.; Supervision, T.W.

DECLARATION OF INTERESTS

The authors declare no competing interests.

Graphical Abstract

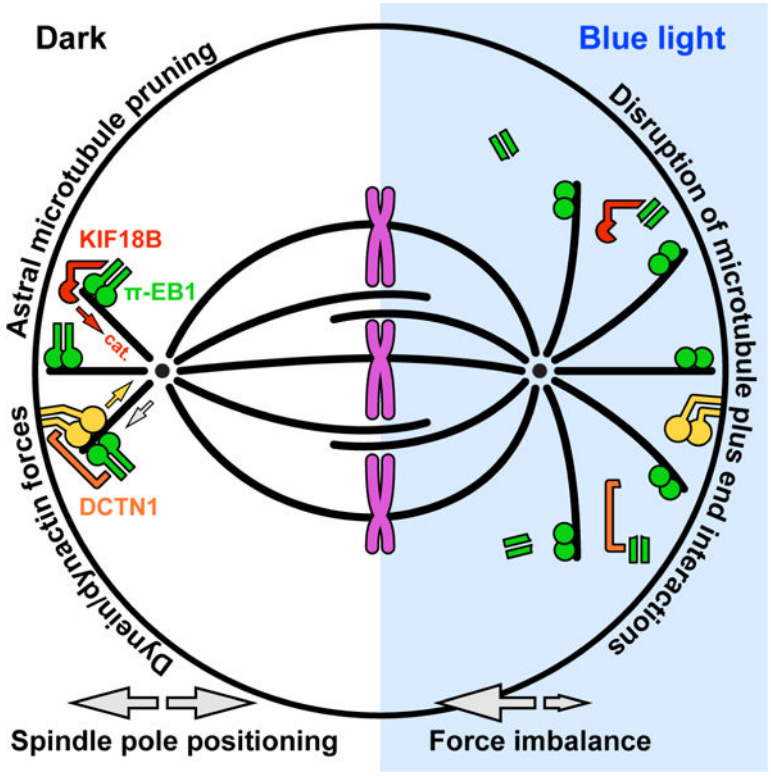

eTOC

Balanced intracellular forces control mitotic spindle shape and position. Dema et al. show that optogenetic inactivation of the +TIP EB1 disrupts this balance, leading to rapid and reversible metaphase spindle shortening. Results highlight EB1 functions in limiting astral microtubule length and in engaging outward pulling forces on spindle poles.

RESULTS AND DISCUSSION

π-EB1 photoinactivation reversibly shortens metaphase spindles

To test how acute inactivation of EB1-mediated +TIP recruitment to growing microtubule (MT) plus ends affects mitotic spindle organization and dynamics, we utilized our previously published H1299 cell line in which the endogenous EB1 and EB3 are removed by CRISPR/Cas9 genome editing and replaced by stable expression of blue light sensitive π-EB1.[7] π-EB1 has its N- and C-terminal domains separated by a LOV2/Zdk1 module resulting in rapid and reversible dissociation of the π-EB1 N-terminal MT- and C-terminal +TIP-binding activities in response to blue light. As expected, mCherry-Zdk1-EB1C associates with growing plus ends of both spindle and astral MTs in the dark and rapidly dissociates from MT ends upon blue light exposure (Figure 1A).

Given that EB1 RNAi in *Drosophila* S2 cells yields shorter spindles[8] and that a fraction of mCherry-Zdk1-EB1C remains at the spindle poles during blue light exposure independent of

MT-binding,[9] we analyzed spindle length in response to acute π-EB1 inactivation. Spindles immediately started to shorten in blue light (Figure 1B; Video S1) indicating an immediate disruption of spindle length maintenance, yet the rate by which spindle length can adjust is limited by spindle and cytoplasm material properties.[2] On average the spindle shortening response was well fitted by a first order exponential decay, which can describe the relaxation response of a viscoelastic material, with a half-life of ~40 seconds (Figure 1C). Using exponential fitting of individual spindle time-lapse sequences to calculate new steady-state lengths during blue light exposure, we found that spindles shortened by ~30% (Figure 1D). In contrast to this metaphase spindle shortening, π-EB1 did not block anaphase spindle elongation (Figure 1E; Video S2). We therefore arrested and enriched cells in metaphase with the proteasome inhibitor MG132 that prevents sister chromatid separation.[10] π-EB1 photoinactivation induced spindle shortening in these metaphase-arrested spindles with similar kinetics (Figure 1C and 1D). However, compared with spindles in cycling cells, MG132-arrested spindles remained slightly longer during blue light possibly because this population is skewed toward metaphase spindles arrested just before anaphase onset or due to proteasome-dependent changes in protein abundance or phosphorylation blocked by MG132 that we did not investigate further.[11]

Nevertheless, because of the more consistent response, we used the MG132 block in most subsequent experiments. Spindle shortening was reversible, and with or without MG132, spindles returned to their original length after blue light exposure (Figure 1C and 1E). In addition, spindles in control cells not expressing π-EB1 did not respond to blue light demonstrating that spindle shortening was not due to phototoxicity (Figure 1C; Figure S2A), but instead is a specific effect of acute EB1 inhibition. Neither inhibition of actomyosin contractility with the Rho-kinase inhibitor Y27632 or a low dose of cytochalasin D that inhibits actin polymerization dynamics in mitosis[12] altered the shortening response (Figure 1D) implying that +TIP-mediated spindle length maintenance is predominantly MT driven. Localized π-EB1 photoinactivation also suggested that both astral and spindle MTs contribute to spindle length maintenance (Figure S1A) although we cannot exclude diffusion of photoinactivated π-EB1 through the cell. Interestingly, spindles in EB1/EB3 -/- cells were not shorter than in control cells (Figure S1C) indicating that genetic loss of EB1 can be compensated and highlights the necessity of acute perturbation to reveal mitotic EB1 functions.

EB1 activity is required for astral microtubule length control

Inhibition of MT dynamics with paclitaxel results in rapid spindle shortening possibly by inhibition of kinetochore (KT)-associated MT assembly while maintaining MT depolymerization near the spindle poles.[13–15] In H1299 cells the kinetics and extent of spindle shortening either with paclitaxel (Figure S1B) or by π-EB1 photoinactivation were remarkably similar. Because π-EB1 photoinactivation inhibits MT growth in interphase,[7] we next asked how π-EB1 photoinactivation affected MT dynamics in mitotic cells. Computational tracking of the fluorescently tagged N-terminus of π-EB1, which remains on MT ends during blue light exposure, revealed that the MT growth rate in metaphase was substantially lower than in interphase.[7] In addition, and in contrast to interphase, the metaphase MT growth rate was only minimally reduced by π-EB1 photoinactivation

(dark: 15.1 +/- 2.3 μm/min; blue light: 14.3 +/- 2.4 μm/min; Figure 2A; Video S3), and not statistically significantly different at the 99% significance level. This indicates that EB1-dependent mechanisms that sustain fast growth of cell body MTs in interphase are absent in mitosis, but also shows that a decrease in MT growth cannot explain the observed spindle shortening phenotype.

To test how EB1 supports spindle MT organization independent of growth rate changes, we observed mCherry-tubulin dynamics in π-EB1 expressing cells. To our surprise and opposite to MT growth inhibition, blue light exposure induced an increase of MTs originating from the spindle poles resulting in an overall 'hairy' appearance even before spindle shortening became apparent (Figure 2C; Video S4). This was reversible and MTs extending into the surrounding cytoplasm disappeared once blue light exposure was terminated. Because the high background of soluble mCherry-tubulin in mitosis makes it difficult to resolve astral MT ends in live cells, we quantified this effect by comparing spindle MTs in cells fixed in the dark and during blue light exposure. In these experiments, in which a lower dose of blue light was delivered to the whole coverslip using a custom-designed LED ring[16] spindle shortening remained reversible after 20 mins of blue light exposure (Figure S2A). Remarkably, compared with cells kept in the dark, both the number and length of astral MTs increased dramatically during blue light exposure with many astral MTs extending to the cell cortex (Figure 2D). While we cannot exclude that unbundling of antiparallel central spindle MTs contributes to this hairy spindle phenotype,[17] the observed increase in astral MT length is very similar to the RNAi phenotype of KIF18B,[18,19] a MT-destabilizing kinesin implicated in astral MT length control in metaphase.[19,20] KIF18B binds to EB1 through a SxIP motif,[20] and indeed, in H1299 π-EB1 cells, KIF18B-mScarlet associated with growing astral MT ends in the dark but was rapidly lost from spindle MTs during blue light exposure ($t_{1/2}$ = 1.3 s, Figure 2E). Thus, although *in vitro* KIF18B can bind MTs independent of EB1,[21] our results demonstrate that KIF18B-mediated astral MT pruning in metaphase requires EB1. In addition to KIF18B, another catastrophe-promoting kinesin, KIF2C (MCAK) contributes to mitotic MT length control[20] and similarly dissociates from growing MT ends as a result of π-EB1 photodissociation although KIF2C remains bound to KTs independent of EB1 (Figure S3A). Such inhibition of catastrophe-promoting activities is further consistent with an increased dwell time of growing astral MT ends at the cortex (Figure 2B).

EB1 is required to engage cortical pulling forces in metaphase

Spindle position is controlled by forces acting on astral MTs by dynein/dynactin localized to the cell cortex.[22] Transition from end-on MT interactions with this cortical force-generating machinery in metaphase to lateral dynein/dynactin-binding along the side of astral MTs in anaphase is thought to increase dynein-mediated forces partially driving anaphase spindle elongation. Indeed, producing lateral MT attachment by flattening cells in metaphase increases spindle length,[23] the opposite of the spindle shortening we observe when inhibiting π-EB1. Consistent with the hypothesis that π-EB1 photoinactivation disrupts astral MT interactions with cortical dynein/dynactin in metaphase, blue light exposure of only one spindle pole in H1299 π-EB1 cells resulted in asymmetric spindle shortening in which the blue light illuminated pole moved away from the cell cortex while the non-illuminated

pole remained unaffected (Figure 3A; Video S5). In addition, while spindle orientation fluctuated randomly in the dark, asymmetric π-EB1 photoinactivation on opposite sides of the pole-to-pole axis near each spindle pole resulted in a spindle rotation bias away from blue light exposed regions (Figure 3B). Although spindle orientation continued to fluctuate randomly after blue light exposure, on average spindles remained in their new positions. Because in these experiments, spindle rotation stopped once spindle poles had moved away from the blue light exposed regions, to test if spindles could be rotated further, we slowly moved wedge-shaped π-EB1 photoinactivation regions on a circular path around the cell cortex. This experiment was technically difficult and only approximately a third of the cells responded clearly to the rotating blue light pattern. However, in the cells that did, the spindle rotation angle followed the rotation ahead of the blue light pattern closely providing further evidence that off-axis π-EB1 photoinactivation generates an imbalance of cortical pulling forces (Figure 3C; Video S5). Of note, resolution in our optogenetics experiments is insufficient to formally distinguish MT interactions with dynein localized to the cell cortex or with dynein in the sub-cortical cytoplasm found in larger cells.[24] Nevertheless, these experiments, together with our data that π-EB1 photoinactivation does not cause anaphase spindle shortening (Figure 1E), demonstrate that EB1 is required to engage the force-generating dynein/dynactin machinery in metaphase, but not in anaphase.

π-EB1 photoinactivation might interfere with cortical pulling forces by two different mechanisms. More and longer astral MTs may physically resist spindle pole movement toward the cortex,[5] or EB1 may be required for dynein/dynactin-mediated cortical MT capture. While we cannot distinguish between these mechanisms and both may be at play, plus end tracking of different dynein subunits in metaphase has been observed.[25] In interphase, the dynactin subunit 1 (DCTN1 or $p150_{Glued}$) can itself be a +TIP, and exists in alternatively spliced variants.[26,27] While the longer neuronal DCTN1 isoform binds MTs directly, in non-neuronal cells part of the basic MT-binding domain is removed reconstituting a cryptic SKLP motif required for binding to EB1 (Figure S3C). Although we were unable to visualize DCTN1 cell cortex localization, the rapid π-EB1 photoinactivation-mediated dissociation of the ubiquitous DCTN1 isoform from growing astral MT ends suggests that in addition to recruiting KIF18B EB1 contributes to productively link dynein/dynactin to growing astral MT ends (Figure S3B). Astral MTs also influence cortical dynein distribution,[28] which may further contribute to the observed spindle positioning phenotypes.

π-EB1 photoinactivation transiently relaxes inter-kinetochore tension

In metaphase, the two KTs of correctly attached chromatid pairs are pulled toward opposite spindle poles and the distance between sister KTs can serve as relative readout of tension across the central spindle.[6,29] Thus, to test how loss of cortical pulling on astral MTs is transmitted through the spindle, we asked how sister KT pairs responded to π-EB1 photoinactivation. Even though this inter-KT distance fluctuates substantially over time, KT pairs in π-EB1 cells frequently appeared to shorten and twist away from the spindle axis during blue light exposure (Fig 4A). Because it was difficult to accurately follow individual sister KT pairs over time, we instead measured the length of as many KT pairs as could be identified in single optical sections at specific time points during blue light exposure. At 3 min, the average KT-KT distance was significantly reduced by ~13% (dark: 0.83 +/-

0.11 μm; blue light: 0.72 +/- 0.11 μm; Figure 4B) indicating that spindles acutely relax in response to disengaging cortical pulling forces. However, this relaxation was transient and normal KT-KT distance was quickly restored in the absence of EB1 activity demonstrating an adaptive response of EB1-independent force generating mechanisms. In addition, KT pairs did not shorten in response to localized π-EB1 photoinactivation of only a small KT population on one side of the spindle (Figure 4C). Together, this implies that EB1 is not directly involved in generating tension across KT pairs even though it is localized to growing ends of KT-MT bundles.[30] However, several EB1-dependent +TIPs including KIF2C, CLASP1/2,[6] and Astrin-SKAP[31] localize to KTs, and indeed π-EB1 photoinactivation impaired accurate chromosome segregation consistent with a role of these +TIPs in KT-MT attachment error correction.[32] 81% of cells (17 out of 21) exhibited chromosome segregation errors when blue light exposure was started at metaphase compared with 31% of control cells (18 out of 58) in the dark (Figure 4E).

Because the duration from nuclear envelope breakdown (NEB) to completion of metaphase increased ~3-fold when π-EB1 H1299 cells were exposed to prolonged lower blue light dose throughout the cell cycle (Figure 4D; Figure S2B), we last asked how π-EB1 photoinactivation affected spindle assembly. When blue light exposure was started during prophase, spindles remained very small, and chromosomes frequently failed to align but instead surrounded a central mini spindle (Figure 4E). While this is consistent with an inhibition of cortical pulling forces, it also indicates additional defects in prometaphase spindle pole separation although EB1 interactions with the antiparallel MT sliding machinery that drives central spindle elongation are not known.[33]

Because accurate chromosome segregation is fundamental to life, redundant systems ensure mitotic spindle fidelity, consistent with the mild mitotic phenotypes of genetic EB1 removal in *Drosophila*[8,34] and the absence of dramatic spindle defects in vertebrate EB1/3 -/- cells (Figure S1C).[35] In contrast, acute optogenetic π-EB1 inactivation reveals EB1 functions that remain hidden in genetic experiments. However, it should be noted that π-EB1 dissociation products may have additional dominant effects and therefore more dramatic consequences than EB1 removal alone. For example, the EB1 C-terminal half could interfere with cortical MT capture, although mCherry-Zdk1-EB1C does not localize to the cortex in blue light. Notably, although MT growth was linked to spindle length,[36,37] π-EB1 photoinactivation-mediated spindle shortening was not accompanied by a MT growth rate decrease. Instead, we think that acute EB1 inhibition causes an imbalance of forces acting on spindle poles that actively drives spindle shortening. To our knowledge, such fast and reversible spindle length change has not previously been reported. Spindles do not shorten during optogenetic inactivation of the MT-bundling protein PRC1.[38] Consistent with pulling on astral MTs, spindles move toward optogenetically recruited NuMa,[39] but also in these experiments spindle length did not change indicating that spindle tension persists. Spindles remained short in π-EB1 H1299 cells in blue light and only returned to their original length when EB1 activity is reinstated, in agreement with slower developmental scaling mechanisms that act through controlling component or MT nucleation site availability.[37,40,41] In conclusion, our results highlight the importance of EB1-mediated MT end interactions in regulating spindle length and position, which in addition to ensuring accurate chromosome segregation[42] have important roles in asymmetric developmental cell divisions.[43]

STAR METHODS

RESOURCE AVAILABILITY

Lead contact—Further information and requests for resources and reagents should be directed to and will be fulfilled by the lead contact, Torsten Wittmann (torsten.wittmann@ucsf.edu).

Materials availability—All unique/stable reagents generated in this study are available from the Lead Contact without restriction. Plasmids will also be deposited with Addgene.

Data and code availability

- All data reported in this paper will be shared by the lead contact upon reasonable request.
- All original code is available in this paper's supplemental information.
- Any additional information required to reanalyze the data reported in this paper is available from the lead contact upon request.

EXPERIMENTAL MODEL AND SUBJECT DETAILS

Cell lines and cell culture—Parental NCI-H1299 human non-small cell lung carcinoma cells (ATCC Cat# CRL-5803, RRID:CVCL_0060, male), or π-EB1 H1299 cells were cultured in RPMI 1640 supplemented with 10% FBS and non-essential amino-acids. Production of π-EB1 H1299 cells is described elsewhere.[7,44] H1299 cell lines were cultured at 37°C, 5% CO_2 in a humidified tissue culture incubator and regularly tested for mycoplasma contamination (IDEXX BioResearch). H1299 cells and sublines were previously authenticated by STR profiling.[7]

METHODS DETAIL

Molecular cloning—The KIF18B coding sequence was amplified by PCR from 24xMoonTag-kif18b-24xPP7 (Addgene plasmid #128604[45] was a gift from Marvin Tanenbaum) and cloned into KpnI and BamHI sites of pCMV-CKAP5-mScarlet-I[7] by Gibson Assembly thereby replacing the CKAP5 ORF with KIF18B.

pEB1N-mApple-LZ-LOV2 was cloned by inserting the mApple and LZ-LOV2 coding sequences into the XhoI and BamHI sites of EB1N-mCherry-LZ-LOV2[7] by Gibson Assembly. mApple and LZ-LOV2 coding sequences were amplified using primers detailed in the key resource table.

mCherry-Dynactin-C-18, representing the neuronal DCTN1 isoform, was obtained from the UCSF Michael Davidson plasmid collection. The alternatively spliced ubiquitous DCTN1 isoform was generated by PCR amplification of the dynactin coding sequence upstream and downstream of the SKLP motif sequence using mCherry-Dynactin-C18 as a template. Resulting PCR amplicons were joined by overlap extension PCR using the two outermost primers. The final PCR product was digested with XhoI and EcoRI and ligated into the XhoI/EcoRI sites of plasmid pBio-mCherry-C1.

All constructs were verified by sequencing and primer sequences are included in the key resources table.

Live cell microscopy and π-EB1 photoinactivation—For microscopy, cells were plated in glass-bottom dishes (Mattek). Cells were arrested in metaphase with 10 μM MG132 (MilliporeSigma) shortly before imaging and were used for a maximum of 4 hours after MG132 addition. 10 μM Y27632 (Tocris Bioscience) was added 2 hours before imaging to inhibit ROCK. 100 nM Cytochalasin D (MilliporeSigma) was added 1 hour before imaging to inhibit f-actin polymerization dynamics. 5 μM paclitaxel (Thermo Fisher) was added during imaging. Spy555-tubulin (Cytoskeleton. Inc) was added to the medium 30 minutes before cell imaging at a 1:2000 dilution from a stock prepared according to the manufacturer's directions. SiR-tubulin (Cytoskeleton. Inc) was employed in a similar fashion at a 300 nM final concentration. Transfection was performed with Lipofectamine 3000 (Thermo Fisher) according to manufacturer's protocol.

Spindle shortening and position experiments were done on a Yokogawa CSU-X1 spinning disk confocal microscopy on a microscope system essentially as described,[46] but upgraded with a more sensitive Prime BSI sCMOS camera (Teledyne Photometrics) with a 60x 1.49 NA oil immersion lens (Nikon). On this microscope, a Polygon 1000 digital micromirror device (Mightex) equipped with a 470 nm LED is coupled into an auxiliary eyepiece camera port on a Ti-E inverted microscope stand (Nikon).[16] Using an 80/20 beamsplitter in the emission lightpath this allows simultaneous confocal imaging and π-EB1 photoinactivation. Blue light exposure regions were drawn on the fly with the PolyScan2 software (Mightex) using a still acquisition as template, except to induce prolonged spindle rotation. In the spindle rotation experiment, a sequence of small triangular regions on opposite sides of the spindle pole axis was pre-programmed in PolyScan2 and rotated around the cell center by 1° every 40 s. For fast time-lapse imaging with acquisition frequencies at or above 1 Hz, blue light exposure was directly triggered by the camera with a 40 ms delay after camera exposure and 10 ms blue light pulses. In experiments with slower time lapse acquisition, the Polygon was triggered with an Arduino microcontroller at 1–2 Hz.

All other Imaging of intracellular dynamics was performed on a newer Yokogawa CSU-W1/SoRa spinning disk confocal system in SoRa mode on a Ti2 inverted microscope stand (Nikon), and images acquired with an ORCA Fusion BT sCMOS camera (Hamamatsu) with 2x2 binning to reduce photobleaching. EB1N-mApple-LOV2 imaging experiments to measure MT growth rates had three phases (20 s image acquisition without blue light exposure, 30 s blue light exposure without image acquisition, and finally 20 s image acquisition with blue light) with images acquired every 0.5 s to capture equilibrium MT dynamics before and during blue light exposure. This system was similarly equipped with a Polygon 1000 (Mightex) through an auxiliary filter turret and LAPP illuminator (Nikon) and integrated control of imaging and photoactivation was through NIS Elements v5.3 software (Nikon).

Lastly, bulk blue light exposure of cells in glass-bottom 12-well plates (Cellvis) for long-term multi-point imaging of cell cycle progression and for analyzing spindle structure in fixed cells was done with a custom-built Arduino-controlled 470 nm LED cube.[16] In all

cases, the minimal blue light dose to achieve π-EB1 photoinactivation was determined by observing dissociation of fluorescently labeled πEB1 C-terminal constructs from growing MT ends.[7]

Immunofluorescence—Microtubule staining was performed as described.[47] In brief, cells grown on coverslips were washed in PBS, fixed in 0.25% glutaraldehyde in 80 mM K-PIPES, 1 mM EGTA, 1 mM $MgCl_2$, then quenched three times in 0.1% $NaBH_4$ in PBS. Fixed cells were permeabilized with 0.3% Triton X-100 in PBS, then blocked in 1% BSA in PBS, and stained with rat anti α-tubulin (Biorad, MCA77G) diluted 1:750 in 0.1% Triton X-100, 1% BSA in PBS.

Image analysis—Spindle length and rotation measurements as well as astral MT number and length quantifications were performed manually in Fiji.[48] Spindle length was determined by measuring the pole-to-pole distance in optical sections and equilibrium spindle length during blue light exposure was determined by fitting the spindle length time-lapse data for each cell with a single exponential decay function using the Curve Fitting toolbox in MATLAB (Mathworks, Inc.).

MT growth rates were measured with u-track essentially as described[7] with the exception that Poisson-distributed shot noise was removed prior to tracking using the NIS Elements v5.3 Denoise.ai neural net (Nikon). In side-by-side comparisons, this resulted in substantial improvement of MT growth track quality. Frame-to-frame MT growth rates were extracted from the tracking results using a custom MATLAB script (instantaneous_vg.m; see Methods S1) and the median of all these instantaneous velocities per cell was calculated to minimize the impact of outlier tracking errors. The u-track particle tracking package for MATLAB is available from the Danuser Lab at http://www.utsouthwestern.edu/labs/danuser/software/.

Sub-resolution distances between sister KTs[6] were measured with a custom MATLAB script (KT_profile.m; see Methods S1), in which two Gaussian functions are fitted along an intensity profile across interactively selected KT pairs in single optical sections.

Images in figures and videos were processed with NIS Elements v5.3 Denoise.ai (Nikon) to reduce shot noise. No non-linear contrast adjustments were made, and images are shown in pseudo-color or contrast-inverted as indicated in the figure legends.

QUANTIFICATION AND STATISTICAL ANALYSIS

Details of statistical analysis including the type of test, p-values and numbers of biological replicates are provided within the relevant figures and figure legends. All statistical analysis was done in MATLAB (Mathworks, Inc.)., and graphs were produced in MATLAB and in Excel (Microsoft). In all figures, box plots show median, first and third quartile, with whiskers extending to observations within 1.5 times the interquartile range. No randomization, stratification or sample size estimation strategies have been employed. Unless indicated otherwise in the text, all data points from a given experiment were analyzed, and a $p < 0.01$ is considered statistically significant. For every experiment reported, at least 3 biological replicates with similar results were performed.

Supplementary Material

Refer to Web version on PubMed Central for supplementary material.

ACKNOWLEDGEMENTS

We thank Marvin Tanenbaum and Michael Davidson for plasmids, Tim Allertz and Samuel Luchsinger Morcelle for help with cloning, Shima Rahgozar for help with cell culture, and the Dumont lab and all members of the HSW-6 community for productive discussions. This work was supported by National Institutes of Health grants R21 CA224194, R01 NS107480, S10 RR026758 and S10 OD028611 to T.W.

REFERENCES

1. Pavin N, and Tolić IM (2016). Self-Organization and Forces in the Mitotic Spindle. Annu. Rev. Biophys 45, 279–298. [PubMed: 27145873]
2. Elting MW, Suresh P, and Dumont S (2018). The Spindle: Integrating Architecture and Mechanics across Scales. Trends Cell Biol 28, 896–910. [PubMed: 30093097]
3. van Haren J, and Wittmann T (2019). Microtubule Plus End Dynamics − Do We Know How Microtubules Grow?: Cells boost microtubule growth by promoting distinct structural transitions at growing microtubule ends. BioEssays 41, 1800194.
4. van der Vaart B, Manatschal C, Grigoriev I, Olieric V, Gouveia SM, Bjelić S, Demmers J, Vorobjev I, Hoogenraad CC, Steinmetz MO, et al. (2011). SLAIN2 links microtubule plus end-tracking proteins and controls microtubule growth in interphase. J. Cell Biol 193, 1083–1099. [PubMed: 21646404]
5. Singh D, Schmidt N, Müller F, Bange T, and Bird AW (2021). Destabilization of Long Astral Microtubules via Cdk1-Dependent Removal of GTSE1 from Their Plus Ends Facilitates Prometaphase Spindle Orientation. Curr. Biol 31, 766–781. [PubMed: 33333009]
6. Pemble H, Kumar P, van Haren J, and Wittmann T (2017). GSK3-mediated CLASP2 phosphorylation modulates kinetochore dynamics. J. Cell Sci 130, 1404–1412. [PubMed: 28232523]
7. van Haren J, Charafeddine RA, Ettinger A, Wang H, Hahn KM, and Wittmann T (2018). Local control of intracellular microtubule dynamics by EB1 photodissociation. Nat. Cell Biol 20, 252–261. [PubMed: 29379139]
8. Goshima G, Wollman R, Stuurman N, Scholey JM, and Vale RD (2005). Length control of the metaphase spindle. Curr. Biol 15, 1979–1988. [PubMed: 16303556]
9. Louie RK, Bahmanyar S, Siemers KA, Votin V, Chang P, Stearns T, Nelson WJ, and Barth AIM (2004). Adenomatous polyposis coli and EB1 localize in close proximity of the mother centriole and EB1 is a functional component of centrosomes. J. Cell Sci 117, 1117–1128. [PubMed: 14970257]
10. Kumar P, Chimenti MS, Pemble H, Schönichen A, Thompson O, Jacobson MP, and Wittmann T (2012). Multisite phosphorylation disrupts arginine-glutamate salt bridge networks required for binding of cytoplasmic linker-associated protein 2 (CLASP2) to end-binding protein 1 (EB1). J. Biol. Chem 287, 17050–17064. [PubMed: 22467876]
11. Kabeche L, and Compton DA (2013). Cyclin A regulates kinetochore microtubules to promote faithful chromosome segregation. Nature 502, 110–113. [PubMed: 24013174]
12. Moore AS, Coscia SM, Simpson CL, Ortega FE, Wait EC, Heddleston JM, Nirschl JJ, Obara CJ, Guedes-Dias P, Boecker CA, et al. (2021). Actin cables and comet tails organize mitochondrial networks in mitosis. Nature 591, 659–664. [PubMed: 33658713]
13. Waters JC, Mitchison TJ, Rieder CL, and Salmon ED (1996). The kinetochore microtubule minus-end disassembly associated with poleward flux produces a force that can do work. Mol. Biol. Cell 7, 1547–1558. [PubMed: 8898361]
14. Dumont S, and Mitchison TJ (2009). Force and Length in the Mitotic Spindle. Curr. Biol 19.

15. Shirasu-Hiza M, Perlman ZE, Wittmann T, Karsenti E, and Mitchison TJ (2004). Eg5 causes elongation of meiotic spindles when flux-associated microtubule depolymerization is blocked. Curr. Biol 14, 1941–1945. [PubMed: 15530396]
16. van Haren J, Adachi LS, and Wittmann T (2020). Optogenetic control of microtubule dynamics. In Methods in Molecular Biology, pp. 211–234.
17. Thomas EC, Ismael A, and Moore JK (2020). Ase1 domains dynamically slow anaphase spindle elongation and recruit Bim1 to the midzone. Mol. Biol. Cell 31, 2733–2747. [PubMed: 32997572]
18. Stout JR, Yount AL, Powers JA, LeBlanc C, Ems-McClung SC, and Walczak CE (2011). Kif18B interacts with EB1 and controls astral microtubule length during mitosis. Mol. Biol. Cell 22, 3070–3080. [PubMed: 21737685]
19. Walczak CE, Zong H, Jain S, and Stout JR (2016). Spatial regulation of astral microtubule dynamics by Kif18B in PtK cells. Mol. Biol. Cell 27, 3021–3030. [PubMed: 27559136]
20. Tanenbaum ME, MacUrek L, Van Der Vaart B, Galli M, Akhmanova A, and Medema RH (2011). A complex of Kif18b and MCAK promotes microtubule depolymerization and is negatively regulated by aurora kinases. Curr. Biol 21, 1356–1365. [PubMed: 21820309]
21. McHugh T, Gluszek AA, and Welburn JPI (2018). Microtubule end tethering of a processive kinesin-8 motor Kif18b is required for spindle positioning. J. Cell Biol 217, 2403–2416. [PubMed: 29661912]
22. Kiyomitsu T (2019). The cortical force-generating machinery: how cortical spindle-pulling forces are generated. Curr. Opin. Cell Biol 60, 1–8. [PubMed: 30954860]
23. Guild J, Ginzberg MB, Hueschen CL, Mitchison TJ, and Dumont S (2017). Increased lateral microtubule contact at the cell cortex is sufficient to drive mammalian spindle elongation. Mol. Biol. Cell 28, 1975–1983. [PubMed: 28468979]
24. Xie J, and Minc N (2020). Cytoskeleton Force Exertion in Bulk Cytoplasm. Front. Cell Dev. Biol 8, 69. [PubMed: 32117991]
25. Schmidt R, Fielmich LE, Grigoriev I, Katrukha EA, Akhmanova A, and van den Heuvel S (2017). Two populations of cytoplasmic dynein contribute to spindle positioning in C. elegans embryos. J. Cell Biol 216, 2777–2793. [PubMed: 28739679]
26. Dixit R, Levy JR, Tokito M, Ligon LA, and Holzbaur ELF (2008). Regulation of dynactin through the differential expression of p150 Glued isoforms. J. Biol. Chem 283, 33611–33619. [PubMed: 18812314]
27. Zhapparova ON, Bryantseva SA, Dergunova LV, Raevskaya NM, Burakov AV, Bantysh OB, Shanina NA, and Nadezhdina ES (2009). Dynactin subunit p150Glued isoforms notable for differential interaction with microtubules. Traffic 10, 1635–1646. [PubMed: 19778315]
28. Tame MA, Raaijmakers JA, Van Den Broek B, Lindqvist A, Jalink K, and Medema RH (2014). Astral microtubules control redistribution of dynein at the cell cortex to facilitate spindle positioning. Cell Cycle 13, 1162–1170. [PubMed: 24553118]
29. Elting MW, Prakash M, Udy DB, and Dumont S (2017). Mapping Load-Bearing in the Mammalian Spindle Reveals Local Kinetochore Fiber Anchorage that Provides Mechanical Isolation and Redundancy. Curr. Biol 27, 2112–2122. [PubMed: 28690110]
30. Tirnauer JS, Canman JC, Salmon ED, and Mitchison TJ (2002). EB1 targets to kinetochores with attached, polymerizing microtubules. Mol. Biol. Cell 13, 4308–4316. [PubMed: 12475954]
31. Kern DM, Monda JK, Su KC, Wilson-Kubalek EM, and Cheeseman IM (2017). Astrin-SKAP complex reconstitution reveals its kinetochore interaction with microtubule-bound Ndc80. Elife 6, e26866. [PubMed: 28841134]
32. Manning AL, Bakhoum SF, Maffini S, Correia-Melo C, Maiato H, and Compton DA (2010). CLASP1, astrin and Kif2b form a molecular switch that regulates kinetochore-microtubule dynamics to promote mitotic progression and fidelity. EMBO J 29, 3531–3543. [PubMed: 20852589]
33. Vukušić K, Ponjavić I, Buđa R, Risteski P, and Tolić IM (2021). Microtubule-sliding modules based on kinesins EG5 and PRC1-dependent KIF4A drive human spindle elongation. Dev. Cell 56, 1253–1267.e10. [PubMed: 33910056]

34. Rogers SL, Rogers GC, Sharp DJ, and Vale RD (2002). Drosophila EB1 is important for proper assembly, dynamics, and positioning of the mitotic spindle. J. Cell Biol 158, 873–884. [PubMed: 12213835]
35. Yang C, Wu J, de Heus C, Grigoriev I, Liv N, Yao Y, Smal I, Meijering E, Klumperman J, Qi RZ, et al. (2017). EB1 and EB3 regulate microtubule minus end organization and Golgi morphology. J. Cell Biol 216, 3179–3198. [PubMed: 28814570]
36. Reber SB, Baumgart J, Widlund PO, Pozniakovsky A, Howard J, Hyman AA, and Jülicher F (2013). XMAP215 activity sets spindle length by controlling the total mass of spindle microtubules. Nat. Cell Biol 15, 1116–1122. [PubMed: 23974040]
37. Rieckhoff EM, Berndt F, Elsner M, Golfier S, Decker F, Ishihara K, and Brugués J (2020). Spindle Scaling Is Governed by Cell Boundary Regulation of Microtubule Nucleation. Curr. Biol 30, 4973–4983. [PubMed: 33217321]
38. Jagrić M, Risteski P, Martinčić J, Milas A, and Tolić IM (2021). Optogenetic control of prc1 reveals its role in chromosome alignment on the spindle by overlap length-dependent forces. Elife 10, e61170. [PubMed: 33480356]
39. Okumura M, Natsume T, Kanemaki MT, and Kiyomitsu T (2018). Dynein–dynactin–NuMA clusters generate cortical spindle-pulling forces as a multiarm ensemble. Elife 7, e36559. [PubMed: 29848445]
40. Good MC, Vahey MD, Skandarajah A, Fletcher DA, and Heald R (2013). Cytoplasmic volume modulates spindle size during embryogenesis. Science (80-.) 342, 856–860.
41. Hazel J, Krutkramelis K, Mooney P, Tomschik M, Gerow K, Oakey J, and Gatlin JC (2013). Changes in cytoplasmic volume are sufficient to drive spindle scaling. Science (80-.) 342, 853–856.
42. Goshima G, and Scholey JM (2010). Control of mitotic spindle length. Annu. Rev. Cell Dev. Biol 26, 21–57. [PubMed: 20604709]
43. Sunchu B, and Cabernard C (2020). Principles and mechanisms of asymmetric cell division. Dev 147.
44. Wittmann T, and van Haren J (2018). Generation of cell lines with light-controlled microtubule dynamics. Protoc. Exch, 10.1038/protex.2017.155.
45. Boersma S, Khuperkar D, Verhagen BMP, Sonneveld S, Grimm JB, Lavis LD, and Tanenbaum ME (2019). Multi-Color Single-Molecule Imaging Uncovers Extensive Heterogeneity in mRNA Decoding. Cell 178, 458–472. [PubMed: 31178119]
46. Stehbens S, Pemble H, Murrow L, and Wittmann T (2012). Imaging intracellular protein dynamics by spinning disk confocal microscopy. Methods Enzymol 504, 293–313. [PubMed: 22264541]
47. Stehbens SJ, Paszek M, Pemble H, Ettinger A, Gierke S, and Wittmann T (2014). CLASPs link focal-adhesion-associated microtubule capture to localized exocytosis and adhesion site turnover. Nat. Cell Biol 16, 558–570.
48. Schindelin J, Arganda-Carreras I, Frise E, Kaynig V, Longair M, Pietzsch T, Preibisch S, Rueden C, Saalfeld S, Schmid B, et al. (2012). Fiji: An open-source platform for biological-image analysis. Nat. Methods 9, 676–682. [PubMed: 22743772]

HIGHLIGHTS

- Light-sensitive π-EB1 allows spatiotemporal analysis of mitotic EB1 functions
- Optogenetic π-EB1 inactivation rapidly and reversibly shortens metaphase spindles
- EB1 functions in astral microtubule pruning without impacting microtubule growth rate
- EB1 is needed to engage dynein-mediated pulling forces on astral microtubules

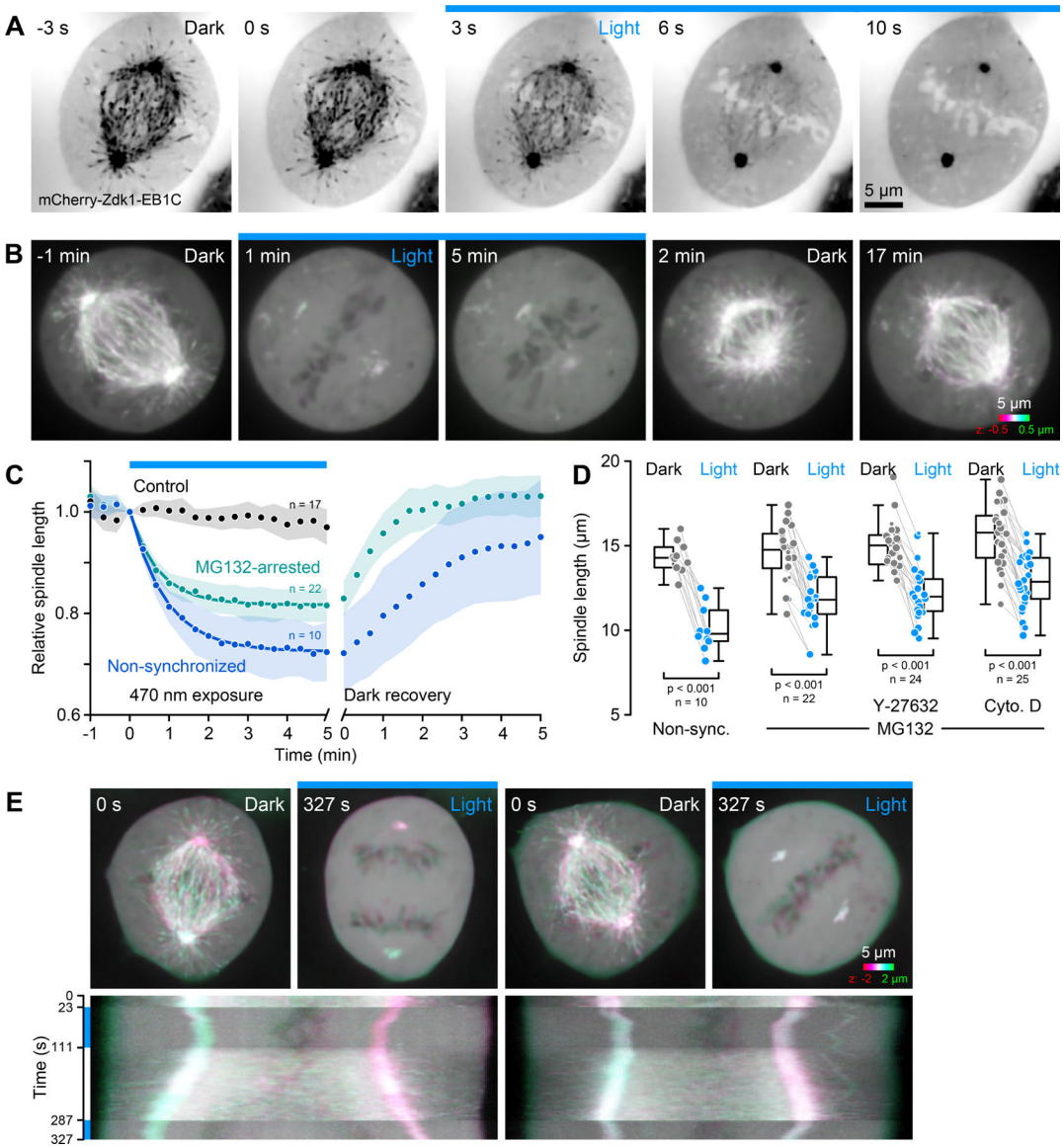

Figure 1. π-EB1 photoinactivation causes rapid and reversible metaphase spindle shortening.

(A) Blue light-mediated rapid dissociation of mCherry-tagged π-EB1C from growing spindle MT ends, but not from spindle poles in a metaphase π-EB1 H1299 cell. Single channel images in this and subsequent figures are shown with inverted contrast for improved visibility. **(B)** Longer time-lapse of a similar cell demonstrating reversible spindle shortening during blue light exposure. Images of z-stacks are color-coded maximum intensity projections to compensate for spindle pole movements out of focus. **(C)** Relative spindle length over time in response to blue light. Shown is the average of the indicated number of cells for each condition. Shaded areas: 95% confidence intervals; solid lines: single exponential fits of the shortening phase. **(D)** Spindle length comparison before and during blue light in the indicated conditions determined by exponential fitting of the individual shortening time series. In this and subsequent figures, box plots show median, first and third quartile, with whiskers extending to observations within 1.5 times the

interquartile range. The size of the individual data points corresponds to the goodness of the fit and grey lines connect data from the same cell. Statistical analysis by paired Student's t-test. **(E)** Color-coded maximum intensity projections of the first and last frames and kymographs along the pole-to-pole axis of a time-lapse sequence of two cells from the same field of view. The cell on the left enters anaphase during the dark recovery phase. Note that anaphase elongation does not stop during a second blue light exposure. Blue bars in all panels indicate time phases with blue light stimulation. See also Figures S1 and S2, and Videos S1 and S2.

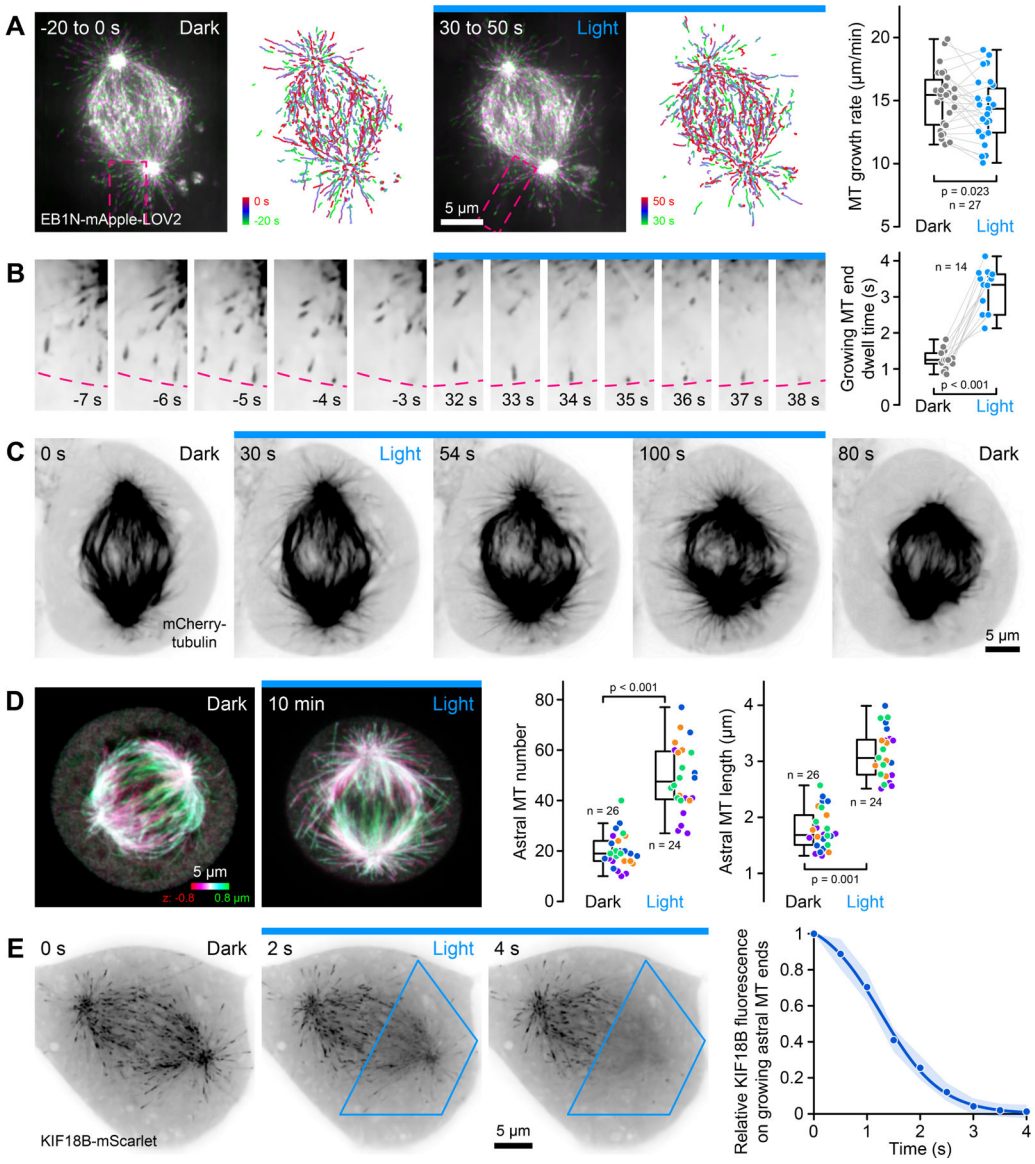

Figure 2. π-EB1 photoinactivation increases astral MT length.

(A) EB1N-mApple-LOV2-labelled MT plus ends before and during blue light exposure in MG132-arrested metaphase spindles. Maximum intensity projections in alternating colors over 20 s at 3-s intervals and MT growth tracks over the same time window illustrate MT growth dynamics before and during blue light exposure. Comparison of the median MT growth rate per cell before and during blue light is shown on the right. **(B)** Time-lapse sequences of the areas indicated in A show that MT ends touching the cell cortex (dashed lines) remain growing for a longer time in blue light exposed cells. This dwell time is quantified on the right. Grey lines connect data from the same cell. Statistical analysis by paired Student's t-test. **(C)** Time-lapse sequence of a π-EB1 H1299 cell expressing mCherry-tagged α-tubulin. Note the increase in astral MT number and length in blue light. **(D)** Color-coded maximum intensity projections of MTs in fixed metaphase spindles in the dark or after 10 min blue light exposure. Box plots show the comparison of astral MT

length and number with colors indicating data from 4 independent experiments. Statistical analysis by unpaired Student's t-test of the experimental mean. See also Figure S2A. **(E)** π-EB1 H1299 cell expressing mScarlet-I-tagged Kif18B in the dark and during local blue light exposure of only the right spindle half. Blue outline indicates the light-exposed area. The graph shows the relative KIF18B-mScarlet fluorescence intensity over time on n = 20 growing astral MT ends from four cells. Shaded area: 95% confidence interval; solid line: logistic fit. Single channel images in B, C and E are shown with inverted contrast, and blue bars in all panels indicate time phases with blue light. See also Figure S3, and Videos S3 and S4.

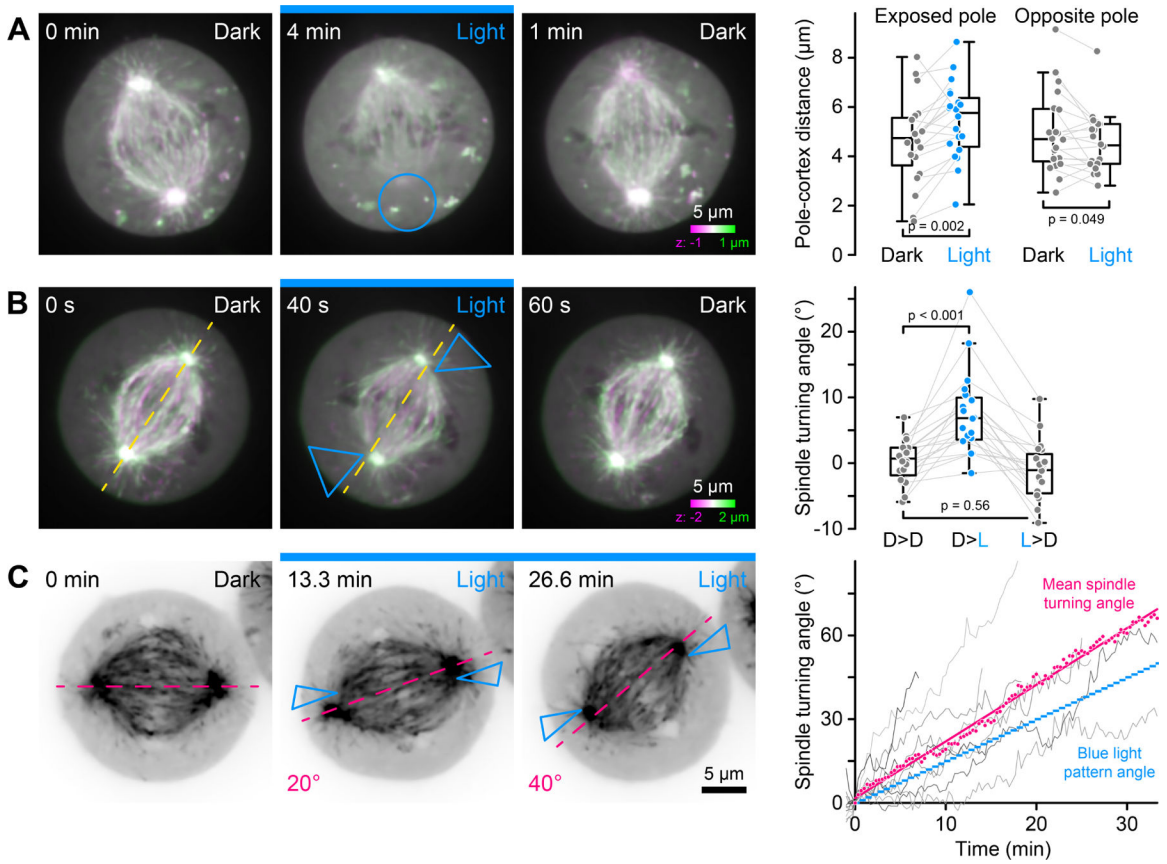

Figure 3. Spindle rotation by local π-EB1 photoinactivation.

(A) Metaphase π-EB1 H1299 cell in which only the lower spindle pole was exposed to blue light. Box plots show the nearest distance of both the light-exposed and the opposite spindle pole from the cortex in the dark and 2 min during blue light (n = 20 cells). Statistical analysis by paired Student's t-test. **(B)** Metaphase π-EB1 H1299 cell with off-axis blue light exposure near both spindle poles. Box plots show the degree of spindle rotation over 1 min intervals in the dark (D>D), when blue light is switched on (D>L), and when blue light is switched off (L>D) with positive angles defined as rotation away from the blue light pattern (n = 20 cells). Statistical analysis by one-way ANOVA and Tukey-Kramer HSD test. **(C)** Metaphase π-EB1 H1299 cell with off-axis blue light pattern rotation by 1° every 40 s. The magenta dashed line shows the expected rotation at the indicated time points. Faster movement of the photoinactivation regions did not result in faster spindle rotation. In the graph, grey lines are the spindle axis rotation of individual cells that responded to the rotation. Magenta symbols are the average rotation of these n = 11 cells with the solid line showing a linear fit. The blue stepped line shows the rotation of the blue light pattern. Images in A and B are color-coded maximum intensity projections, and in C are contrast inverted. All cells were MG132-arrested and localized blue light exposure is indicated by blue outlines. See also Video S5.

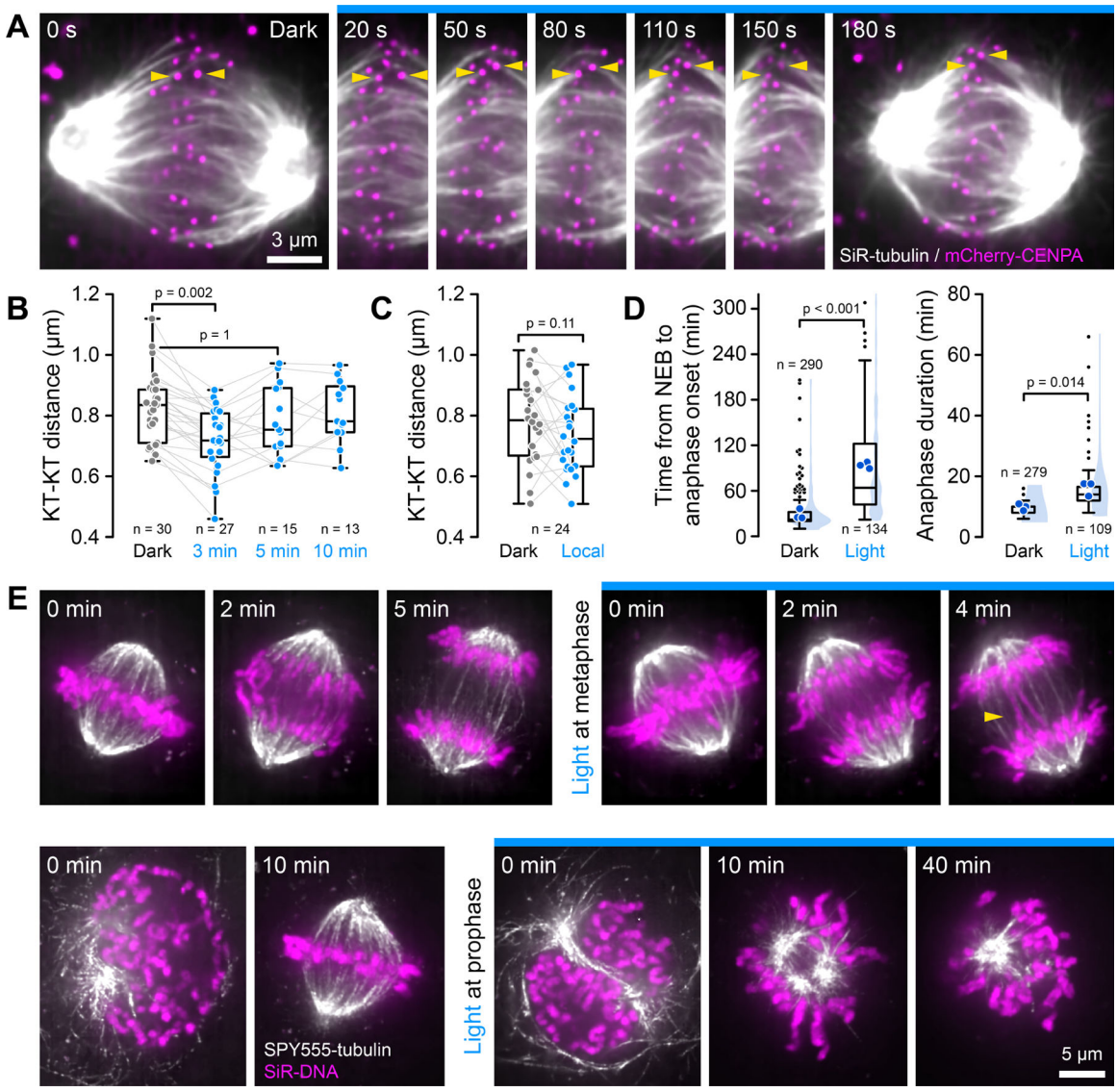

Figure 4. π-EB1 photoinactivation induces transient relaxation of inter-KT tension.

(A) Time-lapse sequence of a metaphase π-EB1 H1299 cell expressing mCherry-CENPA to label KTs. MTs are labeled with SiR-tubulin. Yellow arrowheads highlight a KT pair that visibly shortens during blue light exposure. **(B)** Distance between sister KTs in π-EB1 H1299 metaphase spindles in the dark and at indicated times during blue light exposure. Grey lines connect data points from the same cells but note that not all cells were followed through all time points. Statistical analysis by one-way ANOVA and Tukey-Kramer HSD test indicating significant KT-KT distance shortening only at 3 min. **(C)** Comparison of distance between sister KTs in the dark and after 3 min of local blue light exposure of only a few KT pairs. Statistical analysis by paired Student's t-test. **(D)** Timing of progression through mitosis in π-EB1 H1299 in the dark or exposed to blue light. Blue shaded areas: kernel density distribution of all observed cells from 3 independent experiments. Statistical analysis by unpaired Student's t-test of the experimental mean (dark blue symbols). See Figure S2B for example time-lapse sequences. **(E)** Examples of chromosome segregation

and alignment defects in π-EB1 H1299 cells exposed to blue light either starting at meta- or prophase as indicated compared with control cells that remained in the dark.

KEY RESOURCES TABLE

REAGENT or RESOURCE	SOURCE	IDENTIFIER
Antibodies		
Rat monoclonal anti-Tubulin (clone YL1/2)	Bio-rad	MCA77G (RRID:AB_378785)
Bacterial and virus strains		
NEB 5-Alpha Competent cells	New England Biolabs	C2987H
Chemicals, peptides, and recombinant proteins		
SPY-555 Tubulin	Cytoskeleton Inc.	CY-SC203
SiR-Tubulin	Cytoskeleton Inc.	CY-SC002
SPY-650 DNA	Cytoskeleton Inc.	CY-SC501
MG132	MilliporeSigma	C2211
Y-27632	Tocris Bioscience	Cat. No. 1254
Cytochalasin D	MilliporeSigma	C8273
Paclitaxel	Thermo Fisher	P3456
Critical commercial assays		
Lipofectamine 3000	Thermo Fisher	L3000001
Experimental models: Cell lines		
NCI-H1299	ATCC	CRL-5803
H1299 EB1/EB3 -/-	Previously described[7]	N/A
π-EB1 H1299 EB1/EB3 -/- stably expressing untagged EB1N-LOV2 and EGFP-Zdk1-EB1C	Previously described[7]	N/A
π-EB1 H1299 EB1/EB3 -/- stably expressing EB1N-EGFP-LOV2 and mCherry-Zdk1-EB1C	Previously described[7]	N/A
Oligonucleotides		
KIF18B F 5'-ATCCGCTAGCGCTACCGGACTCAGATCTACCATGGCAGTGGAGGACAGCACGCTGCAAG-3'	This study	N/A
KIF18B R 5'-GATCACTGCCTCGCCCTTGCTCACCATtGGATCCGGACACCTTGGTGACGCCGTTCCCT-3'	This study	N/A
mApple F 5'-CTGGTGTGGTGCGAAAGAACCCTGGTCTCGAGATGGTGAGCAAGGGCGAGGAGAATAAC-3'	This study	N/A
mApple R 5'-TATCTTCCAGCTGTTTCATacctccCTTGTACAGCTCGTCCATGCCGCCGGTGGAG-3'	This study	N/A
gcn4-LOV2 F 5'-ggaggtATGAAACAGCTGGAAGATAAAGTG-3'	This study	N/A
gcn4-LOV2 R 5'-GATTATGATCAGTTATCTAGATCCGGTGGATCCTTAAAGTTCTTTTGCCGCCTCATCAA-3'	This study	N/A
Dynactin F 5'-ggtctcgagctATGAGTACGGAGGCAAGCGCCC-3'	This study	N/A
Dynactin R 5'-GCTGGCTGGGCGAGTAGGCAGTTTGCTGGTCTTTGCAGC-3'	This study	N/A
Dynactin F 5'-GCTGCAAAGACCAGCAAACTGCCTACTCGCCCAGCCAGC-3'	This study	N/A
Dynactin R 5'-accgaattcCAGTTATCTAGATCCGGTGGATCC-3'	This study	N/A

REAGENT or RESOURCE	SOURCE	IDENTIFIER
Recombinant DNA		
EB1N-mApple-LZ-LOV2	This study	N/A
KIF18B-mScarlet-I	This study	N/A
mCherry-KIF2C	Previously described[7]	N/A
mCherry-Dynactin-C-18	Michael Davidson	N/A
mCherry-Dynactin-SKLP motif	This study	N/A
mCherry-α-tubulin	Gia Voeltz	Addgene # 49149
mCherry-CENPA-C-22	Michael Davidson	Addgene # 55015
Software and algorithms		
NIS Elements v5.3	Nikon	https://www.microscope.healthcare.nikon.com/products/software/nis-elements
PolyScan2	Mightex	https://www.microscope.healthcare.nikon.com/products/software/nis-elements
MATLAB R2021a	Mathworks	https://www.mathworks.com/products/matlab.html
u-track	Gaudenz Danuser, Khuloud Jaqaman	https://github.com/DanuserLab/u-track
Fiji	Open Source	https://fiji.sc/
Microsoft Excel	Microsoft	https://www.microsoft.com/en-us/
Adobe Creative Suite	Adobe	https://www.adobe.com/creativecloud.html
Other		
35 mm glass-bottom dishes (No. 1.5 cover glass)	Mattek	P35G-1.5–20-C
12-well glass bottom plate (No. 1.5 cover glass)	Cellvis	P12–1.5H-N